Journal of the Mechanical Behavior of Biomedical Materials 84 (2018) 265–272

Contents lists available at ScienceDirect

Journal of the Mechanical Behavior of Biomedical Materials

journal homepage: www.elsevier.com/locate/jmbbm

Time-elapsed synchrotron-light microstructural imaging of femoral neck fracture☆

Saulo Martelli*, Egon Perilli

Medical Device Research Institute, College of Science and Engineering, Flinders University, 1284 South Road, Clovelly Park, 5042 South Australia, Australia

ARTICLE INFO

Keywords:
Femur microstructure
Time-elapsed synchrotron – light micro-CT imaging
Finite-element
Bone strength
Hip fracture
Biomechanics

ABSTRACT

Time-elapsed micro-computed-tomography (μCT) imaging allows studying bone micromechanics. However, no study has yet performed time-elapsed μCT imaging of human femoral neck fractures. We developed a protocol for time-elapsed synchrotron μCT imaging of the microstructure in the entire proximal femur, while inducing clinically-relevant femoral neck fractures. Three human cadaver femora (females, age: 75–80 years) were used. The specimen-specific force to be applied at each load step was based on the specimens' strength estimated *a priori* using finite-element analysis of clinical CT images. A radio-transparent compressive stage was designed for loading the specimens while recording the applied load during synchrotron μCT scanning. The total μCT scanning field of view was 146 mm wide and 131 mm high, at 29.81 μm isotropic pixel size. Specimens were first scanned unloaded, then under incremental load steps, each equal to 25% of the estimated specimens' strength, and ultimately after fracture. Fracture occurred after 4–5 time-elapsed load steps, displaying sub-capital fracturing of the femoral neck, in agreement with finite-element predictions. Time-elapsed μCT images, co-registered to those of the intact specimen, displayed the proximal femur microstructure under progressive deformation up to fracture. The images showed (1) a spatially heterogeneous deformation localized in the proximal femoral head; (2) a predominantly elastic recovery, after load removal, of the diaphyseal and trochanteric regions and; (3) post-fracture residual displacements, mainly localized in the fractured region. The time-elapsed μCT imaging protocol developed and the high resolution images generated, made publicly available, may spur further research into human femur micromechanics and fracture.

1. Introduction

Femoral neck fractures are a major burden to public health carrying the highest morbidity and mortality rates among fragility fractures (Sernbo and Johnell, 1993; Cummings and Melton, 2002). In this context, micro-computed-tomography (μCT) and mechanical tests have shown a unique potential for studying the femoral microstructure (Baruffaldi et al., 2006), the relationship between bone morphometry, strength (Perilli et al., 2012a; Tassani and Matsopoulos, 2014), micromechanics (Nawathe et al., 2014a, 2014b; Thurner et al., 2006) and their age-related changes (Van Rietbergen et al., 2003). By imaging the bone microstructure during step-wise loading, time-elapsed μCT studies allowed visualizing the micro-architectural displacements in small human bone samples (Nazarian et al., 2006; Perilli et al., 2008), small animal bone samples (Thurner et al., 2006; Szabó et al., 2011) and human spine units (Jackman et al., 2016). Yet, it is unclear how experiments conducted on small bone cores translate to the whole femur (Panyasantisuk et al., 2016). Therefore, time-elapsed μCT imaging of the entire proximal femur during step-wise loading may help in understanding human femur micromechanics. However, no study has yet performed time-elapsed μCT imaging of the entire human proximal femur under load, mainly due to technical limitations.

Time-elapsed μCT imaging of specimens as big as the human proximal femur while inducing fracture to the femoral neck is challenging, because it requires 1) a μCT scanner with a large gantry and detector size providing a suitable working volume and 2) an ad-hoc compressive stage. The field of view has to be large enough to image the entire human proximal femur, which can be 134 mm wide from trochanter to femoral head (Iyem et al., 2014) and approximately 100 mm high from the top of the femoral head to below the lesser trochanter. A pixel size in the order of 20–30 μm ensures that relevant micro-architectural features can be captured, including the thin trabeculae in the order of 100 μm (Perilli et al., 2012b). Scanners capable of doing this are, currently, some synchrotron facilities such as the Imaging and Medical

☆ Manuscript submitted for consideration of publication on the 5th of October 2017. We would like to thank Anton Maksimenko for his invaluable support in conducting the experiment at the Australian Synchrotron. This work was supported by the Australian Research Council [DE140101530] and by the Australian Synchrotron (Clayton, VIC, Australia).

* Corresponding author.
E-mail addresses: saulo.martelli@flinders.edu.au (S. Martelli), egon.perilli@flinders.edu.au (E. Perilli).

https://doi.org/10.1016/j.jmbbm.2018.05.016
Received 11 October 2017; Received in revised form 16 December 2017; Accepted 9 May 2018
Available online 22 May 2018

Beamline (IMBL) of the Australian Synchrotron (Clayton, VIC, Australia) and, with some limitations, industrial CT scanners (e.g., Vtomex, General Electrics, Wunstorf, Germany). Synchrotron facilities (Peyrin et al., 1998) are expected to produce a superior image quality and minimal beam hardening, because of the high flux and monochromatic x-ray beam compared to the lower flux and polychromatic beam used by commercial devices.

Fracturing the femoral neck in human femora using step-wise loading is complex. The compressive stage has to be matched to the available μCT assembly (Jackman et al., 2016), it has to be radio-transparent for minimizing x-ray attenuation and image artefacts (Jackman et al., 2016) and it has to be capable of generating a force inducing fracture to the femoral neck, which may range between 0.9 kN and 14.3 kN for elderly white women (Falcinelli et al., 2014). The latter complicates the determination of incremental load steps to be applied to fracture these specimens, as using the same incremental force for all specimens may either lead to a too early damage and failure of weak specimens, or to a high number of load steps required for fracturing the stronger specimens. This is particularly important when specimen number and imaging time available are limited. Furthermore, during the lengthy (up to four hours long in this experiment) time-elapsed imaging process, it is unclear how bone viscoelasticity may affect the bone mechanics in the entire human femoral epiphyses, as it may cause a decay of the applied load (stress relaxation) and/or affect fracture behaviour. Lastly, the compressive force orientation has to be controlled for inducing fracture in the femoral neck (Cristofolini et al., 2007). To this extent, finite-element analysis of clinical-level CT images may provide estimates of possible fracture location and relative strength (Schileo et al., 2014), which may allow determining a specimen-specific incremental load step to be applied if performed *a priori*, hence facilitating time-elapsed μCT experiments on entire human femoral epiphyses.

Thus, here we present a novel imaging protocol developed for obtaining time-elapsed μCT images of the entire proximal human femur subjected to step-wise loading up to fracture at the IMBL, Australian Synchrotron (Clayton, VIC, Australia).

2. Method

The protocol was developed and tested using three human femora from elderly white women. The amount and type of load to be applied at each load step was calculated *a priori* on a specimen-specific basis, using finite-element analysis of clinical-level CT images. Then, the synchrotron μCT images of the femur, while subjected to a progressive step-wise loading up to fracture and post-fracture, with concomitant force data, were obtained using a dedicated imaging protocol and a custom-manufactured radio-transparent compressive stage.

2.1. Femora

Three femora (Table 1) from three elderly white women (75–80 years of age) with no reported history of fragility fractures were obtained from a dedicated body donation program (Science Care, Phoenix, USA). Samples were received frozen and stored at −20 °C at the Biomechanics and Implants Laboratory of Flinders University (Clovelly Park, South Australia). The primary cause of death included hypertension, chronic obstructive pulmonary disease and Alzheimer. Confirmation of non-reactive serology to major infectious disease (i.e., HBsAg; Anti-HCV; HIV-1/-2) was also obtained. Ethics clearance was granted by the Social and Behavioral Research Ethics Committee (SBREC) of Flinders University (Project # 6380).

Table 1
The donors' age and anthropometric details.

ID	Height (cm)	Weight (kg)	Age (years)	Body mass index (BMI)	BMD (g/cm^2)	T-score
1	145	104.3	80	50	0.42	−3.45
2	155	59.0	76	25	0.56	−2.12
3	178	90.7	75	29	0.28	−4.75

2.2. The compressive stage

The compressive stage was designed to fit the size and weight bearing capacity of the μCT assembly at IMBL and included (1) a radio-transparent compression chamber to minimize X-ray absorption and scatter artefacts, (2) an actuation screw mechanism for imposing displacements to the specimen, (3) a low-friction x-y table to minimize transversal force components, and (4) a 6-degree-of-freedom load cell for measuring the force components at the distal specimen (Fig. 1). The compression chamber was a waterproof aluminium cylinder (203 mm diameter, 3 mm wall thickness), closed by a welded aluminium plate at its bottom, which featured a polyethylene spherically shaped pressure socket, centred, designed to host the femoral head. The specimen-actuator complex included, from bottom to top: the specimen, the specimen holder, the 6-degree-of-freedom load cell, the low-friction x-y table and the screw mechanism. The specimen holder was a 104 mm diameter aluminium potting cup, 60 mm high. The 6-degree-of-freedom load cell (ME-measurement systems GmbH, Hennigsdorf, GE) was placed between the aluminium potting cup and the low-friction x-y table (THK Co., Tokyo, Japan) to minimize the transversal force components acting on the specimen. The vertical displacement of the specimen was actuated by the screw-jack mechanism (Benzlers, Örebro, Sweden) and guided by a vertical rail (SKF Inc., Lansdale, PA, USA). Hence, the compressive stage allowed to apply controlled displacements to the specimen assembly and compressive axial force, while minimizing the transversal force components. The screw-jack stroke was 150 mm, the maximal load 10,000 N and the gear ratio 27:1, which allowed a 0.148 mm vertical displacement per revolution. The load cell capacity was 10,000 N and 500 Nm along each of the three coordinate axes; the nominal maximal measurement error was 0.005% for each force component, provided by the manufacturer. The overall external dimensions of the compressive stage were 245 mm diameter, 576 mm height and 14 kg weight, excluding the sample. The global compliance was 272 ± 31 μm/kN, obtained by replacing the sample with a steel cylinder and measuring the longitudinal force component while actuating the screw-jack mechanism (5 repetitions).

2.3. Load steps determination through finite-element analysis

The load step was defined for each specimen using a well-established procedure based on the finite-element analysis of clinical-level computed-tomography images (Schileo et al., 2014). This procedure has been shown to provide reliable estimates ($R^2 = 0.89$, $p < 0.001$) of the fracture load in human femora, although, subjected to a deformation rate of 2–27.5 mm/s (Schileo et al., 2014), which is a much higher deformation rate than the one occurring during the rather lengthy process of completing time-elapsed μCT experiments. In summary, femora were scanned using a clinical CT scanner (Optima CT660, General Electric Medical Systems Co., Wisconsin, USA), after having been thawed for 24 h at room temperature in a water-proof plastic bag and a double layer of absorbent material to maintain bone moisture. Scanning was conducted using a helical scanning protocol, a tube current of 300 mA and a voltage of 140 kVp. The slice thickness and the in-plane pixel size of the cross-section images were 0.625 mm and 0.7 mm, respectively. A CT densitometry calibration phantom (Mindways Software, Inc., Austin, USA) with five samples of known dipotassium hydrogen phosphate (K2HPO4 equivalent density range: 58.88–157.13 mg cm^{-3}) was scanned with the samples. The femur geometry was extracted from the CT images using a semi-automatic segmentation procedure (Simpleware, Exeter, UK). A finite-element

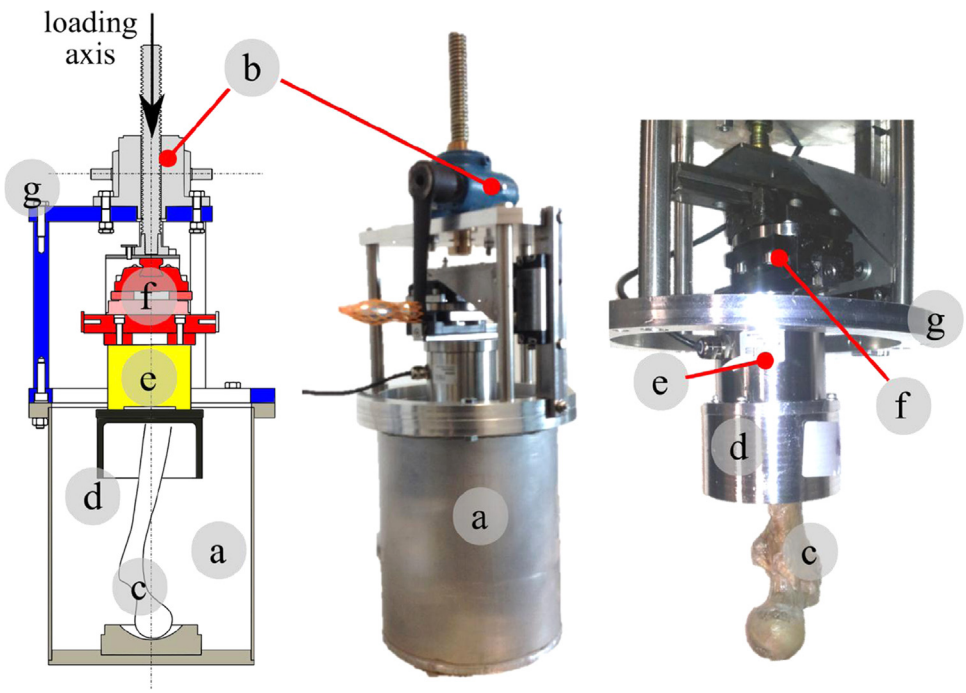

Fig. 1. A schematic representation of the compressive stage (left), the compressive stage assembled (middle) and a detail of the specimen assembly (right). The figure displays the compressive chamber (a), the screw-jack mechanism (b), the femur specimen (c), the aluminium potting cup (d), the load cell (e), the low-friction X-Y table (f) and the structure holding the specimen assembly (g).

mesh was obtained by directly converting the voxels to quadratic hexahedron elements. The element-by-element locally isotropic material properties were defined by (a) calibrating the grey levels in the images to bone density values using the known K2HPO4 densities in the Mindways phantom and (b) using the density-to-elastic modulus relationship reported by Schileo et al. (2014).

The finite-element femur model was fully constrained distally. A nominal force of 1000 N, adducted by 8° from the femoral shaft axis in the coronal plane, was applied to the femoral head. This loading configuration mimics the hip force vector orientation in the one-leg stance configuration (orthoload.com) and it has been shown to induce clinically relevant fracture patterns to the femoral neck (Cristofolini et al., 2007). Nodal strains were calculated using the linear Preconditioned Conjugate Gradient solver implemented in ANSYS (ANSYS Inc., Cannonsburg, USA) and averaged over a 3 mm diameter spherical volume. The estimated fracture load was obtained by scaling the nominal load to match the fracture threshold strain either in tension (0.73% strain) or in compression (1.04% strain) (Schileo et al., 2014).

2.4. Specimen preparation

The femoral diaphysis was cut at 180 mm from the proximal femoral head. The femoral head was centred on the vertical loading axis of the compressive stage, the plane containing the neck and the diaphysis axis was aligned with the frontal plane in the compressive stage and the diaphysis axis was aligned with the vertical loading axis. The specimen was then adducted by 8° (Fig. 1) and potted 55 mm deep in aluminium cups by using dental cement (Soesterberg, The Netherlands), which met the ISO 5833 requirements. This specimen's configuration allowed, once it was mounted on the compressive stage, to align the loading axis in the compressive stage with the hip force vector used in the finite-element analysis.

2.5. Time-elapsed synchrotron-μCT imaging

The femur specimens (after thawing in saline solution for 24 h and then having been fitted on the compressive stage as in point 2.4) were wrapped in fabric tissue soaked with saline solution, sealed in a plastic bag to ensure that bone moisture was maintained throughout the experiment similar to the procedure by Jackman et al. (2016) and mounted on the IMBL's rotation stage for scanning. For each specimen, the first scan was obtained in a zero-load reference position, determined by increasing the vertical load to 100 N and then unloading the specimen until the force profile flattened. Subsequently, the specimen-specific incremental load step was applied, defined for each specimen as a fraction (25%) of its estimated fracture load determined previously via finite-element analysis (point 2.3). At each incremental load step, the load applied to the specimen was increased by manually actuating the screw-jack mechanism while monitoring the longitudinal force component on a laptop computer. For each specimen, step-wise scans were performed up to fracture, followed by one additional post-fracture scan. The 6-degree-of-freedom force components were recorded for the whole duration of the experiment.

Imaging was conducted using the detector Ruby (array size: 2560 × 2160; max FOV: 76.31 × 64.39 mm at 29.81 μm pixel size) and a dedicated off-set scanning mode for extending the FOV to 145.71 mm width at a 29.81 μm pixel size. The x-ray beam, emerging from a rectangular slit, was up to 540 mm in width and 48 mm in height. Scans were performed at 60 keV beam energy, 0.1° rotational increment, 50 μs exposure time, two frames averaging per rotational position. Five consecutive stacked scans were acquired using 5 incremental vertical shifts (26 mm each) of the specimen, resulting in a total height of the imaged volume of 131.37 mm, which included the sample from the femoral head (proximally) to the femoral diaphysis (distally) and the top border of the aluminium potting cup. The 145.71 mm width of the imaged volume was obtained by scanning two batches of 180° rotation each, with the specimen centred 8 cm off-axis (i.e., the off-set scanning mode). The total scanning time was 25.2 min per load step. Each of the 1800 projection images (2560 × 896 pixels in size, 76.31 × 26.71 mm, width × height) representing the entire specimen, was then obtained by stitching horizontally the two images taken in the off-set scanning mode and vertically those from the 5 vertical scans using a custom-routine provided by IMBL. Hence, the final projection images were each 4407 × 4888 pixels in size (131.37 × 145.71 mm, height × width), saved in 32 bit format, floating point, occupying 160 GB disk space. The cross-section image reconstruction was performed using dedicated software available at IMBL resulting in a stack of 4407 cross-section images (4888 × 4888 pixels in size) per load step, for a total volume of

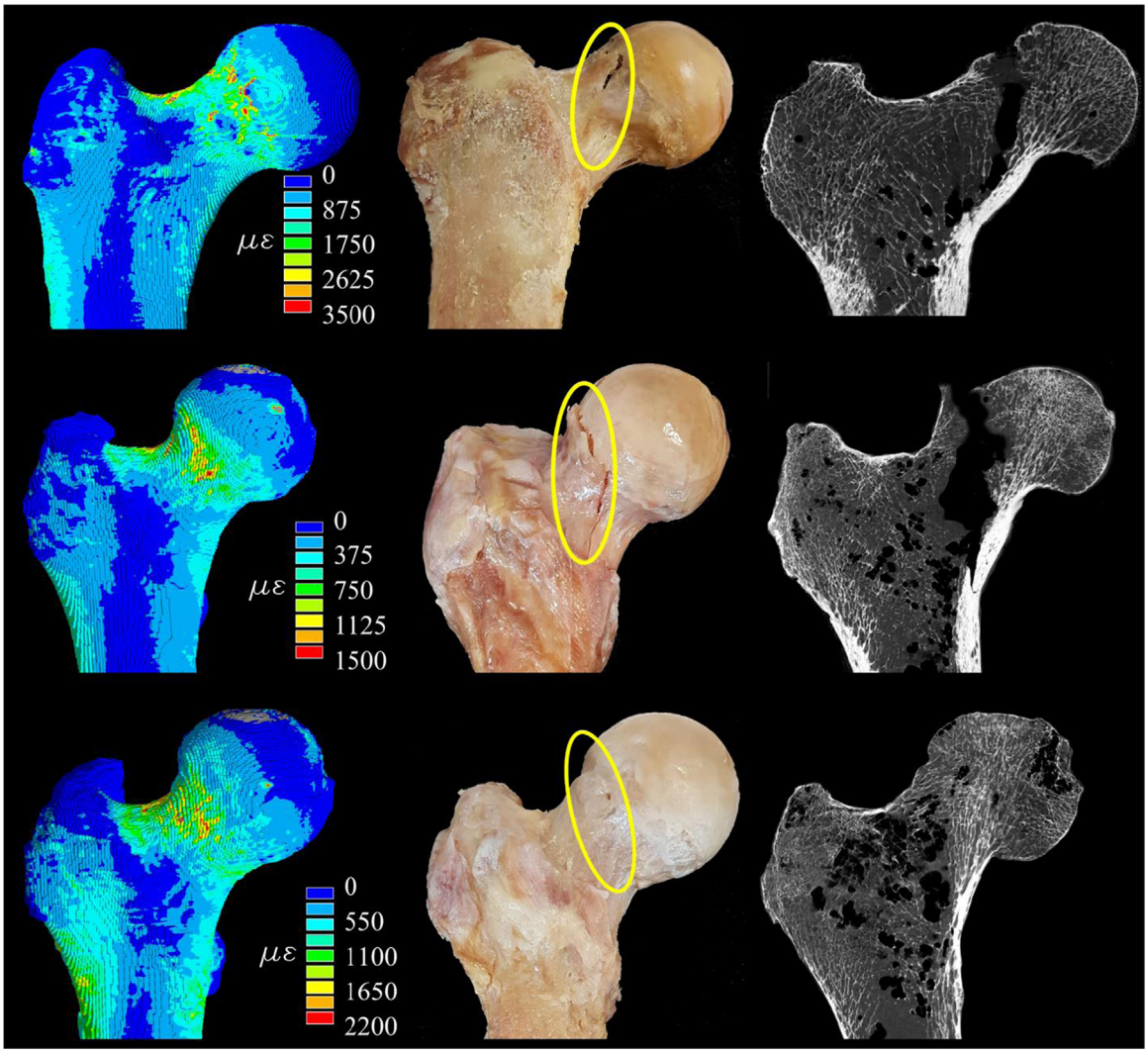

Fig. 2. For each specimen, the principal strain map calculated using finite-element analysis (first column), a photo depicting the superficial fracture pattern highlighted within a yellow ellipse (middle column) and the internal fracture pattern visualized over a coronal cross-section image taken from the synchrotron μCT image dataset, showing the internal microstructure (right column, 29.81 pixel size). (For interpretation of the references to color in this figure legend, the reader is referred to the web version of this article.).

131.37 mm height, 145.71 × 145.71 mm width. The reconstructed images were filtered (3 × 3 Gaussian filter) and stored in external hard-drives (32 bit, floating point, tiff format files) occupying 392 GB disk space per load step.

2.6. Analysis of clinical-level CT images, of the force-time history and of the μCT images

The suitability of the protocol for studying femur mechanics in elderly women was assessed by comparing the range of bone quality (Bone Mineral Density, BMD) across specimens with that in elderly white women (Kanis et al., 2000), the observed fracture pattern with clinically relevant fracture patterns (Pauwel, 1934; Ruedi and Murphy, 2000), by visualizing the trabecular and cortical bone displacements at micro-architectural level and by comparing the measured force to earlier studies of bone viscoelastic response (Sasaki et al., 1993).

The total hip Bone Mineral Content (BMC), BMD and the corresponding osteoporosis level (T-score) were estimated from the clinical CT scans following the guidelines by Khoo et al. (2009) and classified following the World Health Organization guidelines (Kanis et al., 2000). The observed femoral fracture patterns were compared with typical patterns of femoral neck fractures using the classification proposed by Pauwel (1934) and the more recent classification by Ruedi and Murphy (2000).

The time-elapsed 2D and 3D μCT visual representations of the entire proximal femur were first created by subsampling the cross-section images by four, to reduce the computational time. The image datasets of the femur at the various load steps and post-fracture were spatially co-registered to those taken in the initial zero-load condition (reference images) using the rigid registration algorithm implemented in Dataviewer (Skyscan–Bruker, Kontich, Belgium) and a region of the distal end of the specimen as reference volume (cube, 20 mm side). 3D models were created by binarizing the images with bone as a solid (uniform threshold (Perilli et al., 2007)) (CT Analyser, Skyscan–Bruker, Kontich, Belgium) and then visualized (Paraview, Kitware, Clifton Park, NY, USA). Then, the deformation of the femoral epiphysis was analysed by co-registering the full resolution images (29.81 μm) at the height of the lesser trochanter. Cortical and trabecular displacements were visualized by targeting (zooming-in) the analysis of the cross-section images to the region between the femoral head and the lesser trochanter, where the fracture was expected to occur. A public repository was created to allow access to the images to the broad research community (Martelli and Perilli, 2016).

The force relaxation behaviour of the femur was studied by fitting,

to the measured force-time history, the Kohlrausch-Williams-Watts (KWW) function, describing the fast stress relaxation behaviour occurring immediately after load application (Sasaki and Yoshikawa, 1993):

$$\frac{\Delta F(t)}{\Delta F0} = e^{-(t/\tau)^{\beta}}; t = [0, 30]; \quad (1)$$

where ΔF(t) is the load step increment at time t, ΔF0 is the load step increment at time zero, τ and β are the time constant and the shape factor (Sasaki and Yoshikawa, 1993). In the present study, the force-time history was collected for 30 min after application of the load, separated into single load steps, aligned in time by defining time t = 0 at the time of load step application and normalized to the actual load increment. The time constant τ and the shape factor β were then calculated by fitting the KWW function to the normalized force profile.

3. Results

Specimens were all osteoporotic (total hip BMD: 0.28–0.56 g/cm^2; T-score = −4.75 to −2.12) according to the WHO guidelines (Kanis et al., 2000) (Table 1). The three fractured specimens consistently showed a cervical fracture opening in the proximal sub-capital neck, which progressively narrowed moving medially to an incomplete fracture ending in the medial neck (Fig. 2). The observed fracture patterns resembled fracture types II and III according to Pauwel (1934) and type 31-B according to Ruedi and Murphy (2000).

The applied load step was 27.4% ± 0.4% (average ± standard deviation) of the estimated fracture load (range: 3306–5246 N) for each femur. The corresponding load step ranged between 906 N and 1414 N across specimens, with fracture obtained after 4–5 time-elapsed imaging load steps. The finite element analysis predicted the highest load to fracture for specimen #2, followed by #1 and #3 and this order was confirmed experimentally by the magnitude of the actual peak force measured, which followed the same specimen order (#2, #1, #3) (Table 2). Also, the fracture patterns, observed visually on the fractured specimens and by μCT, were consistent with regions subjected to high principal tensile strains in the finite-element analysis (Fig. 2).

The stack of reconstructed μCT cross-section images displayed, starting from the top end, the polyethylene pressure socket, the entire proximal femur, the distal diaphysis embedded in the aluminium cup and the trabecular and cortical bone micro-architecture subjected to an increasingly deformed state, up to fracture (Figs. 3–5). The full-resolution time-elapsed μCT images displayed a spatially heterogeneous deformation of the proximal femur, localized in the proximal head (from the proximal sub-capital to the most medial head region) and the displacement under load of the trabeculae (Fig. 3).

Fig. 4 displays the sequence of coronal cross-section images of a representative specimen (#1) unloaded and then followed by progressively deformed states up to fracture, with the polyethylene pressure socket displacing the superior femoral head. Fig. 5 shows 3D representations of a deformed proximal femur (rendering of 2 mm thick volume, coronal view) at the load step before fracture (~ 81% of the estimated fracture load, white colour), superimposed to a scan in the unloaded reference condition (orange colour); a concomitant lowering and movement towards the medial side of the femoral head and of the superior and inferior neck can be observed, as well as of the greater trochanter and the femoral shaft, compared to the zero-load conditions, with appreciable deformations, as large as fractions of millimetres (Fig. 5b). After fracture (Fig. 5c), the cortical bone of the femoral shaft, and the cortical and trabecular bone of the greater trochanter, recovered most of the displacement observed under load by returning to their original zero-load position, consistent with a predominantly elastic recovery after load removal. Instead, the fractured femoral head and parts of the trabecular and cortical bone in the neck in proximity to the fracture surface remained visibly displaced (lowered), even after load removal.

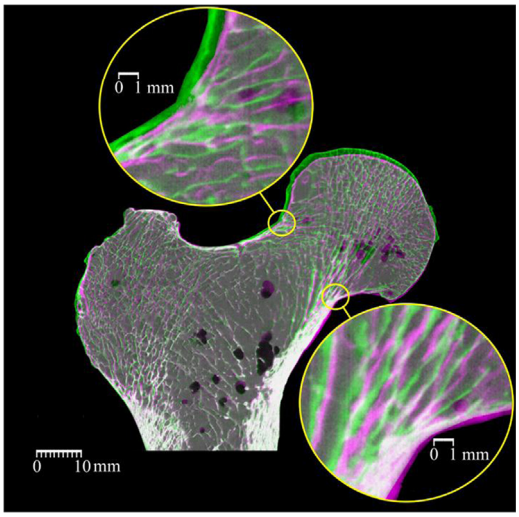

Fig. 3. The microstructure of the proximal femur displaced under load (load step 4) displayed over a coronal synchrotron μCT cross-section image (29.81 pixel size) for one representative specimen (#1). White regions represent bone regions where bone is present before and after load application, green regions represent bone regions where bone is present only in the images of the specimen subjected to no load and pink regions represent bone regions where bone is present when deformed under load. The image shows the highest displacements localized in the superior femoral head indicating high deformation levels as compared to other bone regions. (For interpretation of the references to color in this figure legend, the reader is referred to the web version of this article.).

Table 2
The fracture experiment.

Specimen ID	1	2	3
Estimated fracture load (N) via FE	3788	5246	3306
Measured peak force (N)	3146	3528	2331
Force increment (N) applied per load step[a]	1049 ± 105	1414 ± 119	906 ± 124
Force increment (%) applied per load step[b]	28 ± 2.8%	27 ± 2.3%	27 ± 3.7%
Force relaxation @30 min (N)[a]	526 ± 221	941 ± 401	640 ± 71
Force relaxation @30 min (%)[c]	50 ± 21	67 ± 28	71 ± 11
Steps to fracture (planned)	4	4	4
Applied load steps before fracture	4	4	5

[a] Average value ± SD.
[b] Values are expressed as percentages of the estimated fracture load.
[c] Values are expressed as percentages of the applied load step.

Between load steps, specimens displayed stress relaxation behaviour showing, on average, a decrease of the recorded force by 33% of the applied load step after 7 min (i.e., the average waiting time for scanning to commence after load step application) and by 61% after 30 min (i.e., at scan completion for each load step). The force relaxation behaviour at each load step was well described (R^2 = 0.99, $p < 0.001$) by the KWW function (Sasaki and Yoshikawa, 1993). The range of the time constant and of the shape factor were 50.9–158 min and 0.388–0.443 respectively. Fig. 6 shows the six degree of freedom force measured at the distal end of the femur for specimen #1.

4. Discussion

The aim of this study was to obtain time-elapsed microstructural μCT images of the entire proximal femur under load while inducing fracture to the femoral neck. A novel protocol was designed and successfully applied at the Australian Synchrotron (Clayton, VIC, Australia). Time-elapsed μCT images of the entire proximal femur were obtained for three specimens from elderly white female donors,

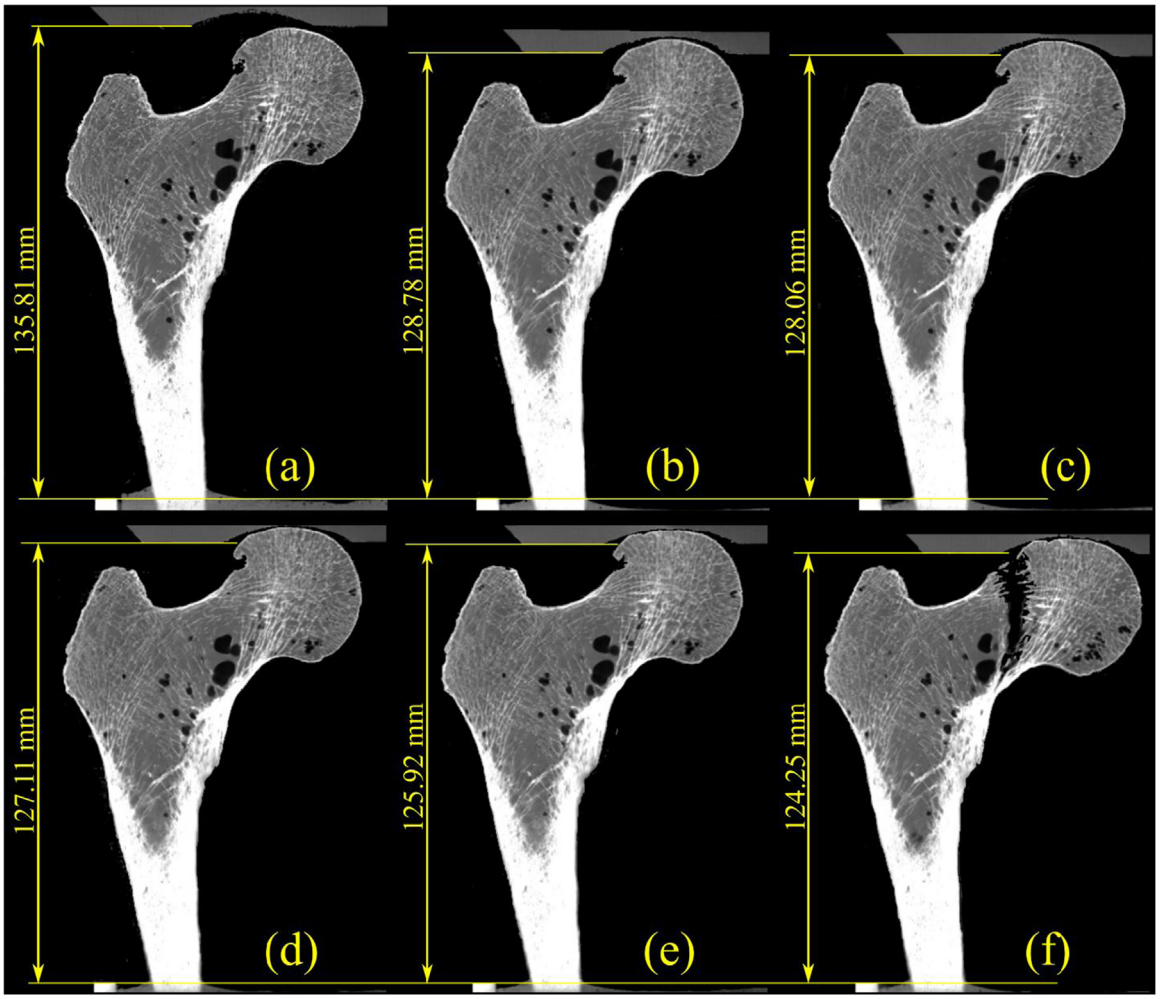

Fig. 4. The time-lapsed μCT images displaying the progressively increasing deformation state of one representative specimen (#1) including no deformation (a), increasingly deformed states (b–e) and after fracture (f). The top border of the specimen holder, the pressure socket and their distance at each load step (in mm) are also visible.

showing the progressive displacement of the femoral microstructure under a step-wise load increase and post-fracture. Moreover, we successfully used finite-element analysis from clinical-level CT scans for planning the time-elapsed imaging experiment, allowing the determination of a specimen-specific load step to be applied and consistently predicting high strains over the experimentally observed fracture region. Therefore, the protocol and the high resolution images generated in the present study can be used to study the deformation and fracture mechanism in human femora.

The images displayed the progressive displacement under load of the femoral microstructure in the whole metaphysis (Figs. 3–5), at a pixel size (29.81 μm) that allows capturing relevant features of bone microstructure (Nazarian et al., 2006; Perilli et al., 2008), a spatially heterogeneous displacement and deformation under load in the proximal femur, and post-fracture residual displacement after load removal, which was mainly localized in the fractured region. Thus, the present study provides a protocol for time-elapsed μCT imaging of the human proximal femur and μCT images for studying trabecular and cortical micromechanics in the entire proximal femur. The conjunct availability of the μCT images and the force-time history can be used for studying the relationship between bone micro-morphometry, deformation and fracture (Baruffaldi et al., 2006; Nawathe et al., 2014a, 2014b; Perilli et al., 2012b) while inducing clinically relevant fractures to the femur. For example, digital volume correlation analysis can be applied to these μCT image datasets, for quantification of volumetric bone strain (Roberts et al., 2014; Jackman et al., 2016) and enabling validation of micromechanical models of the human femur toward advanced surrogates of real samples (Niebur et al., 2000; Taylor et al., 2017). Whereas the latter was beyond the aim of the present study, the time-elapsed μCT images are being made available to the bone research community through an open access policy (Martelli and Perilli, 2016), which may help overcoming the intrinsic difficulties for accessing the limited number of imaging facilities where the present protocol can be implemented.

The step-wise compressive loading, planned *a priori* using finite-element analysis and then experimentally applied using the developed compressive stage, consistently induced clinically relevant sub-capital fractures (Pauwel, 1934; Ruedi and Murphy, 2000). Importantly, the specimens' strength predicted via finite element analysis of clinical-level CT images, which varied substantially from 3306 N to 5246 N across specimens, allowed to rank the specimens according to their estimated strength, enabling a specimen-specific determination of the load step to be applied (906–1414 N) and limiting the number of complete load steps before fracture between 4 and 5 (Table 2). Therefore, finite-element analysis may help planning time-elapsed experiments of entire bone segments of variable strength. Nevertheless, there was a substantial difference between the estimated fracture load and the peak force measured during the time-elapsed experiment attributable to force relaxation (i.e., 50–71% decay of the applied load step over thirty minutes from load step application; Table 2). The force

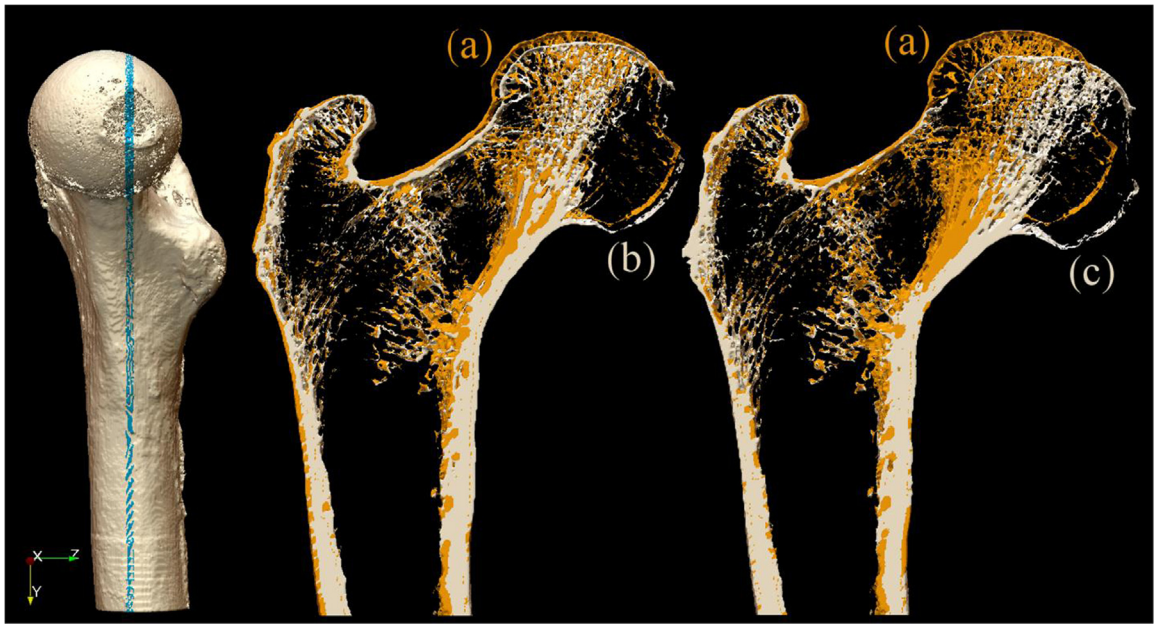

Fig. 5. The 3D geometry of a 2 mm thick stack of coronal synchrotron μCT cross-section images of the specimen subjected to no load (a), after application of the fourth load increment (b) and after fracture (c). The 3D bone geometry of the entire specimen and the location of the 2 mm slice (blue stripe) are displayed on the left. (For interpretation of the references to color in this figure legend, the reader is referred to the web version of this article.).

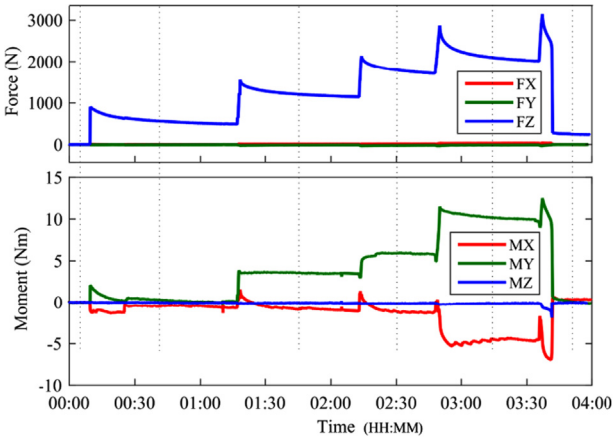

Fig. 6. The six component force measured for one representative femoral specimen (#1). The graph displays the load step sequence up to fracture and the load time history between steps. (For interpretation of the references to color in this figure legend, the reader is referred to the web version of this article.).

relaxation constants reported in the present study (i.e., time constant: 50.9–158 min; shape factor: 0.388–0.443) differ from those previously reported for bovine cortical cores (i.e., time constant: 26–44 min; shape factor: 0.49–0.63)(Sasaki and Yoshikawa, 1993) and similarly showed large inter-specimen variability, particularly for the time constant, likely attributable to inter-specimen differences in tissue mechanics. Hence, the present findings may help planning of future time-elapsed experiments, as well as facilitating the development of viscoelastic models of human femoral mechanics. Finally, the consistency between the fracture patterns observed here using step-wise loading and those observed in previous works using the same loading condition but at much higher loading rates (2–27.5 mm/s (Schileo et al., 2014)) suggests a similarity between the failure modes across different loading rates. This is key in translating results from time-elapsed experiments to real-case scenarios (e.g., impact loading), although more specimens tested to fracture are necessary to confirm this hypothesis.

To the best of our knowledge this is the first study providing time-elapsed microstructural μCT images of the proximal femur while inducing clinically relevant fractures to the femoral neck. The fracture patterns observed in the proximal femur are in agreement with previous experimental results, where the same loading configuration was found to induce a range of clinically relevant fracture patterns from sub-capital to intertrochanteric fractures (Cristofolini et al., 2007). A previous study performed synchrotron light μCT imaging of one femoral epiphysis in unloaded condition at 22.5 μm pixel size, proving the feasibility to visualize the trabecular and cortical bone microarchitecture with a spatial resolution typically used for morphometric analysis on biopsies (Baruffaldi et al., 2006). The pixel size obtained in the present study (29.81 μm) will allow similar analyses (Perilli et al., 2012b) with the advantage to put it in relation to step-wise loading, up to fracture. Several studies used commercially available high-resolution peripheral quantitative computed-tomography (HR-pQCT) for microstructural imaging of the entire human femur (Nawathe et al., 2014a, 2014b; Van Rietbergen et al., 2003), although none of these studies has obtained time-elapsed images of the femur under progressive loading, because the big size (width, length) and the high strength of the human femora prevents imaging and concomitant loading within the compressive stages typically fitting those scanners. In fact, time-elapsed μCT imaging studies of entire human bone segments based on HR-pQCT systems are limited to thoracic vertebrae scanned while compressed using an ad-hoc device (Jackman et al., 2016), conceptually similar to that used in the present study. This study has overcome these technical constraints, by designing a novel ad-hoc compressive stage and performing μCT scans at the Australian Synchrotron, which has a beamline (IMBL) and a detector capable of producing images of big size (145.7 × 145.7 mm), at high resolution (29.81 μm, isotropic). Also, the pixel size in the present images is smaller than that used with the above commercial systems (i.e., 61.5– 80 μm (Nawathe et al., 2014a; Nawathe et al., 2014b; Van Rietbergen et al., 2003)), providing a superior representation of the bone microarchitecture, in a bigger field of view (Perilli et al., 2012b). While technological advances in commercial μCT scanners may allow time-elapsed μCT studies of human femora at some stage in future, at this point in time the open access policy used in the present study (Martelli and Perilli, 2016) will facilitate further research by allowing access to the images to the broad research community.

One limitation of the present study is that the observed fracture patterns, which systematically opened in the proximal sub-capital neck

to end in the medial calcar region, represent a fraction of the fracture patterns typically observable in the clinics (Pauwel, 1934; Ruedi and Murphy, 2000). Most likely, different loading scenarios, loading rates and more specimens tested to fracture would have resulted in a broader range of fracture patterns (Cristofolini et al., 2007). For example, sideways fall loading would have caused a sudden, predominantly compressive state in the upper neck (Nawathe et al., 2014b) as opposed to the quasi-static predominantly tensile state obtained in the present study, likely resulting in a different fracture mode. However, increasing the number of loading conditions and specimens was limited by imaging time available. Furthermore, the fracture behaviour observed in the present study may be affected by a non-physiological load transfer between the spherically shaped polyethylene pressure socket and the femur specimen through the soft soaked fabric layer. However, the load transfer system used in the present study compares favourably with earlier studies using spherical metallic shells (Zani et al., 2015) and a PMMA layer (Ariza et al., 2015) directly in contact with femoral head causing similar fracture patterns to those obtained here and supporting the validity of the present protocol. Lastly, it is important to highlight that time-elapsed scans of specimens of this size, at this high spatial resolution, generate correspondingly large datasets during scanning (for example, 160 GB per load step in this study) and image reconstruction (392 GB per load step), making the following image post-processing and data analysis a computationally intensive task (Perilli et al., 2012b). Therefore, experiments of this kind and the type of analysis to be performed need to be carefully planned *a priori*, considering the resources available in terms of time, operators and computer hardware and software capabilities.

Concluding, the protocol developed enables obtaining time-elapsed synchrotron-light μCT images of the entire human proximal femur under load, while inducing clinically relevant fractures to the femoral neck. The images showed progressive displacement of the femur cortical and trabecular microstructure at a pixel size typically obtainable only on smaller bone segments or small biopsies. The study shows also the usefulness of finite-element analysis on clinical-level CT scans in the planning phase of time-elapsed imaging experiments of this kind for specimens of various strengths, for determining the actual incremental load to be applied at each load step. The time-elapsed μCT images obtained for three elderly white women can be used to study femoral micromechanics and fracture. The public availability of the image datasets (Martelli and Perilli, 2016) will facilitate overcoming the intrinsic difficulties of accessing the limited number of imaging facilities available for conducting similar experiments. This protocol may also provide basis for time-elapsed μCT studies of specimens of similar size, from various skeletal sites under load.

Appendix A. Supplementary material

Supplementary data associated with this article can be found in the online version at http://dx.doi.org/10.1016/j.jmbbm.2018.05.016.

References

Ariza, O., Gilchrist, S., Widmer, R.P., Guy, P., Ferguson, S.J., Cripton, P.A., Helgason, B., 2015. Comparison of explicit finite element and mechanical simulation of the proximal femur during dynamic drop-tower testing. J. Biomech. 48, 224–232. http://dx.doi.org/10.1016/j.jbiomech.2014.11.042.

Baruffaldi, F., Bettuzzi, M., Bianconi, D., Brancaccio, R., Cornacchia, S., Lanconelli, N., Mancini, L., Morigi, M.P.P., Pasini, A., Perilli, E., Romani, D., Rossi, A., Casali, F., 2006. An innovative CCD-based high-resolution CT system for analysis of trabecular bone tissue. IEEE Trans. Nucl. Sci. 53, 2584–2590. http://dx.doi.org/10.1109/TNS.2006.876047.

Cristofolini, L., Varini, E., Viceconti, M., 2007. In-vitro method for assessing femoral implant-bone micromotions in resurfacing hip implants under different loading conditions. Proc. Inst. Mech. Eng. Part H J. Eng. Med. 221, 943–950. http://dx.doi.org/10.1243/09544119JEIM278.

Cummings, S.R., Melton, L.J., 2002. Epidemiology and outcomes of osteoporotic fractures. Lancet 359, 1761–1767. http://dx.doi.org/10.1016/S0140-6736(02)08657-9.

Falcinelli, C., Schileo, E., Balistreri, L., Baruffaldi, F., Bordini, B., Viceconti, M., Albisinni, U., Ceccarelli, F., Milandri, L., Toni, A., Taddei, F., 2014. Multiple loading conditions analysis can improve the association between finite element bone strength estimates and proximal femur fractures: a preliminary study in elderly women. Bone 67, 71–80. http://dx.doi.org/10.1016/j.bone.2014.06.038.

Iyem, C., Güvençer, M., Karatosun, V., Unver, B., 2014. Morphometric evaluation of proximal femur in patients with unilateral total hip prosthesis. Clin. Anat. 27, 478–488. http://dx.doi.org/10.1002/ca.22245.

Jackman, T.M., Hussein, A.I., Curtiss, C., Fein, P.M., Camp, A., De Barros, L., Morgan, E.F., 2016. Quantitative, 3D visualization of the initiation and progression of vertebral fractures under compression and anterior flexion. J. Bone Miner. Res. 31, 777–788. http://dx.doi.org/10.1002/jbmr.2749.

Kanis, J.A., Johnell, O., Oden, A., Jonsson, B., De Laet, C., Dawson, A., 2000. Risk of hip fracture according to the world health organization criteria for osteopenia and osteoporosis. Bone 27, 585–590. 〈http://www.ncbi.nlm.nih.gov/pubmed/11062343〉 (Accessed 8 September 2016).

Khoo, B.C.C., Brown, K., Cann, C., Zhu, K., Henzell, S., Low, V., Gustafsson, S., Price, R.I., Prince, R.L., 2009. Comparison of QCT-derived and DXA-derived areal bone mineral density and T scores. Osteoporos. Int. 20, 1539–1545. http://dx.doi.org/10.1007/s00198-008-0820-y.

Martelli, S., Perilli, E., 2016. Time-Lapsed Microstructural Images of Femoral Neck Fractures in Elderly Caucasian Women. 〈http://dx.doi.org/10.4226/86/592680cb25f8b〉.

Nawathe, S., Nguyen, B.P., Barzanian, N., Akhlaghpour, H., Bouxsein, M.L., Keaveny, T.M., 2014a. Cortical and trabecular load sharing in the human femoral neck. J. Biomech. 48, 816–822. http://dx.doi.org/10.1016/j.jbiomech.2014.12.022.

Nawathe, S., Akhlaghpour, H., Bouxsein, M.L., Keaveny, T.M., 2014b. Microstructural failure mechanisms in the human proximal femur for sideways fall loading. J. Bone Miner. Res. 29, 507–515. http://dx.doi.org/10.1002/jbmr.2033.

Nazarian, A., Stauber, M., Zurakowski, D., Snyder, B.D., Müller, R., 2006. The interaction of microstructure and volume fraction in predicting failure in cancellous bone. Bone 39, 1196–1202. http://dx.doi.org/10.1016/j.bone.2006.06.013.

Niebur, G.L., Feldstein, M.J., Yuen, J.C., Chen, T.J., Keaveny, T.M., 2000. High-resolution finite element models with tissue strength asymmetry accurately predict failure of trabecular bone. J. Biomech. 33, 1575–1583. http://dx.doi.org/10.1016/S0021-9290(00)00149-4.

Panyasantisuk, J., Pahr, D.H., Zysset, P.K., 2016. Effect of boundary conditions on yield properties of human femoral trabecular bone. Biomech. Model. Mechanobiol. 15, 1043–1053. http://dx.doi.org/10.1007/s10237-015-0741-6.

Pauwel, F., 1934. Der Schenkenholsbruck em mechanisches problem, Gd. Des Heilungsvorganges Progn. Und Kausale Ther. Stuttgart, Ger. Ferdinand Engke.

Perilli, E., Baruffaldi, F., Visentin, M., Bordini, B., Traina, F., Cappello, A., Viceconti, M., 2007. MicroCT examination of human bone specimens: effects of polymethylmethacrylate embedding on structural parameters. J. Microsc. 225, 192–200. http://dx.doi.org/10.1111/j.1365-2818.2007.01731.x.

Perilli, E., Baleani, M., Ohman, C., Fognani, R., Baruffaldi, F., Viceconti, M., 2008. Dependence of mechanical compressive strength on local variations in microarchitecture in cancellous bone of proximal human femur. J. Biomech. 41, 438–446. http://dx.doi.org/10.1016/j.jbiomech.2007.08.003.

Perilli, E., Briggs, A.M., Kantor, S., Codrington, J., Wark, J.D., Parkinson, I.H., Fazzalari, N.L., 2012a. Failure strength of human vertebrae: prediction using bone mineral density measured by DXA and bone volume by micro-CT. Bone 50, 1416–1425. http://dx.doi.org/10.1016/j.bone.2012.03.002.

Perilli, E., Parkinson, I.H., Reynolds, K.J., 2012b. Micro-CT examination of human bone: from biopsies towards the entire organ. Ann. Ist. Super. Sanita 48, 75–82. http://dx.doi.org/10.4415/ANN_12_01_13.

Peyrin, F., Salome, M., Cloetens, P., Laval-Jeantet, A.M., Ritman, E., Rüegsegger, P., 1998. Micro-CT examinations of trabecular bone samples at different resolutions: 14, 7 and 2 μm level. Technol. Health Care 6, 391–401. 〈http://www.ncbi.nlm.nih.gov/pubmed/10100941〉 (Accessed 6 December 2016).

Roberts, B.C., Perilli, E., Reynolds, K.J., 2014. Application of the digital volume correlation technique for the measurement of displacement and strain fields in bone: a literature review. J. Biomech. 47, 923–934. http://dx.doi.org/10.1016/j.jbiomech.2014.01.001.

Ruedi, T.P., Murphy, W.M., 2000. Principles of Fracture Management. Thieme, Stuttgart.

Sasaki, N., Yoshikawa, M., 1993. Stress relaxation in native and EDTA-treated bone as a function of mineral content. J. Biomech. 26, 77–83.

Sasaki, N., Nakayama, Y., Yoshikawa, M., Enyo, A., 1993. Stress relaxation function of bone and bone collagen. J. Biomech. 26, 1369–1376. http://dx.doi.org/10.1016/0021-9290(93)90088-V.

Schileo, E., Balistreri, L., Grassi, L., Cristofolini, L., Taddei, F., 2014. To what extent can linear finite element models of human femora predict failure under stance and fall loading configurations? J. Biomech. 47, 3531–3538. http://dx.doi.org/10.1016/j.jbiomech.2014.08.024.

Sernbo, I., Johnell, O., 1993. Consequences of a hip fracture: a prospective study over 1 year. Osteoporos. Int. 3, 148–153. http://dx.doi.org/10.1007/BF01623276.

Szabó, M.E., Taylor, M., Thurner, P.J., 2011. Mechanical properties of single bovine trabeculae are unaffected by strain rate. J. Biomech. 44, 962–967. http://dx.doi.org/10.1016/j.jbiomech.2010.12.008.

Tassani, S., Matsopoulos, G.K., 2014. The micro-structure of bone trabecular fracture: an inter-site study. Bone 60, 78–86. http://dx.doi.org/10.1016/j.bone.2013.12.007.

Taylor, M., Perilli, E., Martelli, S., 2017. Development of a surrogate model based on patient weight, bone mass and geometry to predict femoral neck strains and fracture loads. J. Biomech. 121–127. http://dx.doi.org/10.1016/j.jbiomech.2017.02.022.

Thurner, P.J., Wyss, P., Voide, R., Stauber, M., Stampanoni, M., Sennhauser, U., Müller, R., 2006. Time-lapsed investigation of three-dimensional failure and damage accumulation in trabecular bone using synchrotron light. Bone 39, 289–299. http://dx.doi.org/10.1016/j.bone.2006.01.147.

Van Rietbergen, B., Huiskes, R., Eckstein, F., Ruegsegger, P., 2003. Trabecular bone tissue strains in the healthy and osteoporotic human femur. J. Bone Miner. Res. 18, 1781–1788.

Zani, L., Erani, P., Grassi, L., Taddei, F., Cristofolini, L., 2015. Strain distribution in the proximal human femur during in vitro simulated sideways fall. J. Biomech. 48, 2130–2143. http://dx.doi.org/10.1016/j.jbiomech.2015.02.022.